ASSESSMENT OF MECHANICAL PROPERTIES OF HUMAN HEAD TISSUES FOR TRAUMA MODELLING

Estivaliz Lozano-Mínguez [a*], Marta Palomar [a], Diego Infante-García [b], María José Rupérez [a], Eugenio Giner [a]

[a] Department of Mechanical Engineering and Materials - CIIM, Universitat Politècnica de València, Camino de Vera s/n, 46022 Valencia, Spain

[b] Department of Mechanical Engineering, Universidad Carlos III de Madrid, Avda. de la Universidad 30, 28911, Leganés (Madrid), Spain

* Corresponding authors: eslomin@upv.es

ABSTRACT

Traumatic Brain Injury (TBI) is a serious public health problem worldwide, since it leads to a large number of permanent disabilities and deaths. Extensive research has been conducted in recent years to understand the development of head injury, although further knowledge improvement is required in order to reduce accidental injuries. The accuracy of numerical models when predicting human head behaviour, and hence skull fracture or brain damage, strongly depends on the proper definition of constitutive equations and damage models. However, many discrepancies are found in the literature regarding the constitutive models for head tissues as well as the values of the constants involved in the constitutive equations. Prevention of head injuries and the design of head protections require the statement of damage threshold levels in terms of biomechanical parameters. Therefore, the main goal of this research is to perform a critical review of constitutive models and damage indicators describing human head tissues response under impact loading. A 3D finite element human head model has been generated using computed tomography images, which has been validated through the comparison to experimental data in the literature. The threshold values of the skull and the scalp that lead to fracture have been analysed. We conclude that: 1) compact bone properties are critical in skull fracture, 2) the elastic constants of the CSF

affect the intracranial pressure distribution, and 3) the consideration of brain tissue as a nearly-incompressible solid with a high (but not complete) water content offers pressure responses consistent with the experimental data.

KEYWORDS

Human head model, head tissues, skull fracture, intracranial pressure, head impact response.

1. Introduction

Traumatic Brain Injury (TBI) is defined as an induced structural lesion and/or physiological alteration of brain function due to an external force. It is classified as open (also called penetrating) or closed depending on whether the skull is fractured or not. TBI is considered a severe public health problem worldwide, since it affects over 10 million people annually leading to either death or permanent disabilities [1]. Nearly 35% of TBIs are due to falls, 17% are caused by motor vehicle traffic accidents, about 17% are attributable to sports or work place related injuries, 10% are due to violence, and another 21% are due to unknown causes [2]. Moreover, the World Health Organization (WHO) declares that the world's health community must pay attention to TBI and that many countries need to carry out epidemiologic studies to develop effective preventive methods [3]. Therefore, much research has been conducted over the last decades to understand the development of a head injury and so help to reduce the damage under an impact.

On the other hand, finite element (FE) modelling is a powerful tool widely used to understand and predict the injury mechanisms [4,5]. As in any other FE analysis, the predicted mechanical behaviour of the head is strongly dependent on the constitutive properties of the involved tissues. However, estimating these properties is a great challenge, since these cannot be obtained by means of in vivo tests on humans. In vivo impact experiments carried out on a variety of animal species, such as those performed by Bolander et al. [6] and Li et al. [7], offer a good alternative to monitor the physiologic response, but there is a lack of an adequate scaling law [8]. Besides, the main drawback with post-mortem human tests is that the characteristics of the tissues are altered once blood supply has ceased. Furthermore, although the preservation of tissues prior to

testing plays an important role on the characterization of their mechanical properties, the morphological variation among subjects and the testing type (either quasi-static or dynamic and type of loading) may significantly influence the values of the elastic constants registered [9]. Consequently, it is possible to find many discrepancies between the values of these properties in the literature, e.g. the elastic modulus of the mandibular trabecular bone ranges from 6.9 up to 199.5 MPa [10]. Prevention of head injuries and designing of head protections against impacts, ballistic projectiles or explosive blasts require the statement of damage threshold levels in terms of biomechanical parameters, which should not be reached. Therefore, the objective of this research is to perform a critical review of constitutive models and damage indicators describing human head tissues response under impact loading. To this end, a realistic 3D FE human head model has been constructed from the computed tomography (CT) images of a real human head. This model has been used to simulate some experimental impact tests, aiming to show those properties that (given our numerical model) provide a response closest to reported experimental tests. This 3D FE human head model will enable the analysis of the TBI produced under different scenarios, for example in helmet impacts or accident reconstruction.

To the best of the authors' knowledge, no previous study has compared different mechanical properties with the same FE model simulating experimental impact tests.

2. Development of the 3D FE human head model

2.1. Numerical model description

The head model has been generated from CT images provided by the Hospital Universitari i Politècnic La Fe, from an anonymous middle-aged male subject (see Fig. 1). These medical images were imported into ScanIP v4.2 [11] for segmentation and meshing of the human head FE model. A resample to 0.5 mm/pixel has been performed to obtain the same resolution in x, y and z in order to improve the FE mesh quality and to decrease the required memory.

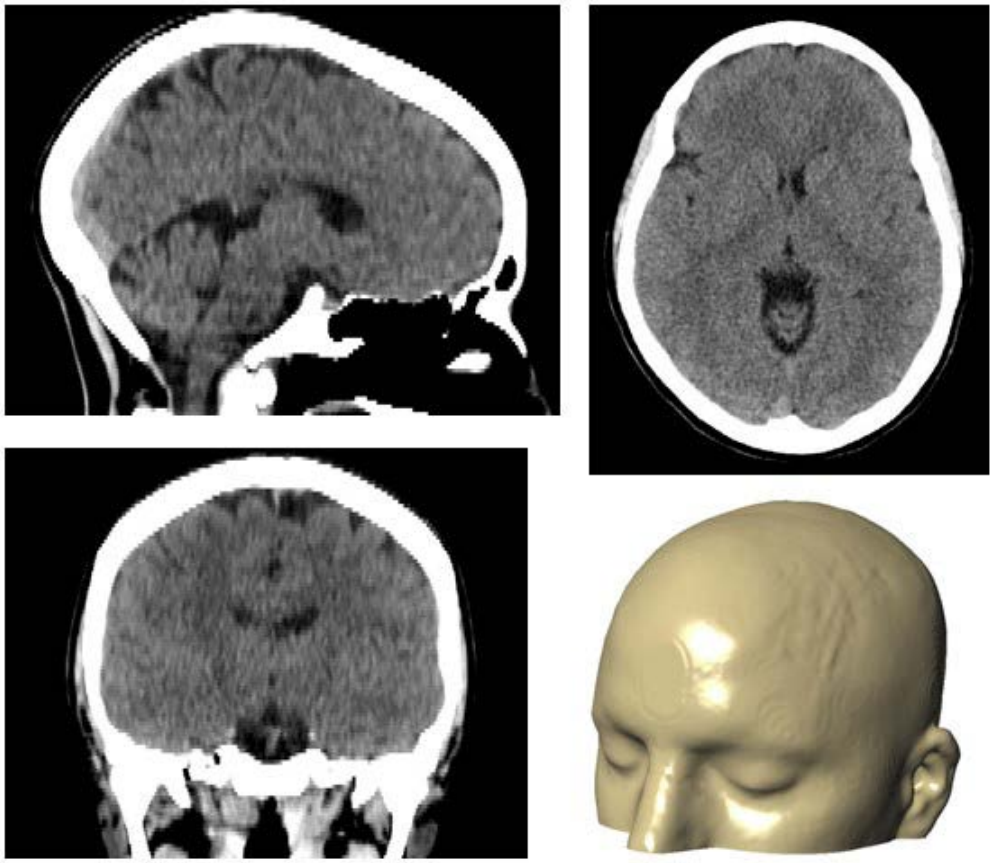

Fig. 1. CT images from an anonymous middle-aged male subject from ScanIP used for the FE model.

In addition to being a vulnerable part of the human body, the human head is an extremely complicated structure and, therefore, several geometrical and material behaviour approximations have been used for years. Following the features of some established head models, our model consists of six differentiated layers: scalp, compact bone, diploë, face bone, cerebrospinal fluid (CSF) and brain, as it can be seen in Fig. 2. The scalp is about 5.3 mm thick at the forehead and about 5.8 mm thick at the vertex; which represents as a whole the hair-bearing skin, subcutaneous connective tissue, epicranial aponeurosis, loose areolar tissue, and pericranium. The skull has been divided in three parts: compact bone (inner and outer tables), diploë (or cancellous bone), and face bones. Thickness and curvature of skull vary substantially depending on the area and among individuals. The frontal thickness of the skull of this subject is about 10 mm thick, while the vertex thickness is about 13 mm. The meninges are composed of three thin membranes: dura mater, arachnoid mater, and pia mater, and covers the brain and spinal cord. The subarachnoid space, laid between the arachnoid mater and the pia mater, is filled with the circulating CSF and contains many fibrous filaments (trabeculae) that connect the two layers and prevent excessive

movement of the brain. Therefore, the CSF layer, structurally representing this set of tissues, has been modelled to cushion the brain from the mechanical shock and to enable relative motion between the skull and the brain, and it is about 2 mm thick. Although structurally the brain may be divided into three parts: cerebrum, cerebellum, and brainstem, it has been considered as a single part since their mechanical properties may be homogenized reducing the computational cost without compromising the accuracy of the results [12,13]. Unlike other models that use membrane or shell elements combined with solid elements, all parts of our model were meshed using solid elements. The mesh is continuous avoiding to use tie constraints, and elongated or distorted elements. Continuum models are preferable since they allow to estimate local phenomena [14]. The FEA software ABAQUS/CAE [15] has been used for the simulation setup and the linear tetrahedral C3D4 element type has been chosen for the 379550-element mesh. These elements have been selected because it is advocated to use the centroid kinematic formulation and a linear combination of stiffness and viscous hourglass control in impact eroding problems using Abaqus/Explicit due to the large localized deformations [16]. Boundary conditions vary according to the simulation, so they will be defined in later sections.

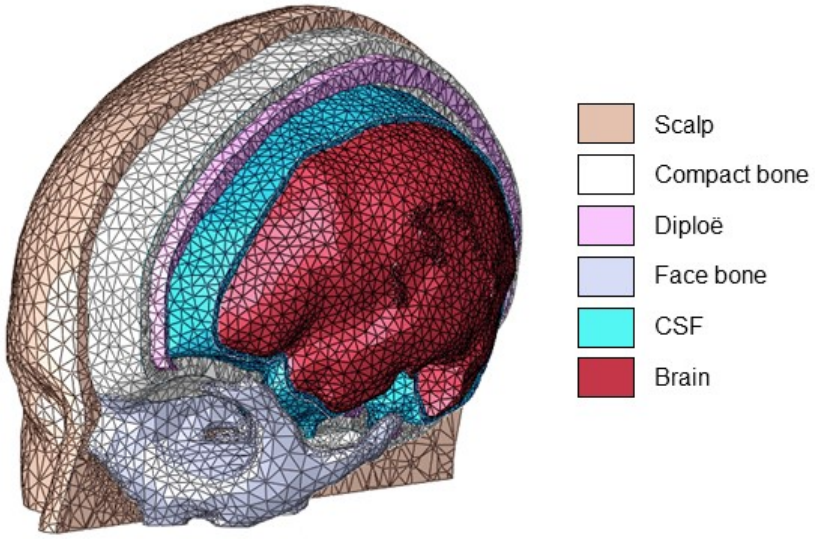

Fig. 2. Human head FE model developed in this work from CT images of Fig.1.

2.2. Material properties review

The majority of human head models agree on adopting a linear-elastic behaviour to model the skull and the scalp [12,17–21]. Earlier FE models considered the brain tissue as a linear-elastic material [18,22–24], while recent studies adopted linear viscoelastic material laws combined with

large-deformation theory [12,14,20,25–27] or nonlinear viscoelastic materials under large deformations [28], the latter being less common. In addition, the most advanced models have considered brain anisotropy [29]. Regarding CSF, there is no conformity to adopt a material constitutive law. Some FE models assumed linear-elastic material constitutive laws for the CSF [12,20,23,26,29–31], while other studies modelled the CSF as a viscoelastic material [32,33] or as a hydrostatic fluid by using a surface-based fluid modelling method [18,19,27,34].

In this work, the mechanical properties of five previous FE human head models have been considered for comparison. Table 1 shows that, in addition to using different material behaviour laws, the values of the elastic constants of the different tissues of the head vary considerably, as mentioned in the introduction section. For example, the Young's modulus of the CSF varies from 0.012 MPa [12] to 1.49 MPa [20] as well as the Young's modulus of both the compact bone and the face bone that ranges from approximately 5,000 MPa [23] to 15,000 MPa [35].

Table 1. Material properties.

		MP1 Gilchrist and O'Donoghue [23]	**MP2 Ruan et al.[20]**	**MP3 Kleiven [35]**	**MP4 Kang et al. [12]**	**MP5 Tse [25]**
Compact Bone	Density (kg m^{-3})	3000	3000	2000	1800	1210
	E (MPa)	5465	12200	15000	15000	8000
	Poisson's ratio	0.22	0.22	0.22	0.21	0.22
Diploë	Density (kg m^{-3})	1750	1750	1300	1500	1210
	E (MPa)	2864	5660	1000	4500	8000
	Poisson's ratio	0.22	0.22	0.22	0.22	0.22
Face	Density (kg m^{-3})	2100	2100	2000	3000	1210
	E (MPa)	5000	5000	15000	5000	8000
CSF	Density (kg m^{-3})	1040	1040	1000	1040	1040
	E (MPa)	0.1845	1.49	1.26	0.012	1.314
	Poisson's ratio	0.499	0.489	0.4999	0.49	0.4999
Brain	Density (kg m^{-3})	1040	1040	1040		1140
	Elastic constants	Elastic E=0.558 MPa, υ=0.485	Elastic E=0.307 MPa, ν =0.4996	Hyperelastic* C_{10}=62 Pa C_{01}=69 Pa	Elastic $K = \frac{E}{3(1-2\nu)}$ =1.125 GPa	Elastic ν =0.48
	Viscoelastic constants**	-	g_1=0.682 τ_1=0.02857	g_1=0.636 g_2=0.363 τ_1= 0.008 τ_2=0.15	g_1=0.659 τ_1=0.00689	g_1=0.68182 τ_1=0.028571
Scalp	Density (kg m^{-3})	1200 [36]	1300 [37]	1130	1200	1130
	E (MPa)	16.7	16.7	16.7	16.7	16.7
	Poisson's ratio	0.42	0.42	0.42	0.42	0.42

* Constants refer to the Mooney-Rivlin model as described in Abaqus User's Manual [15]
** Constants refer to the Prony Series model as described in Abaqus User's Manual [15]

The first model selected for our study was developed by Gilchrist and O'Donoghue [23] to investigate the dynamic response of the human head after being subjected to direct translational

impacts. Therein, all head tissues were modelled as linear-elastic materials. The main conclusion from this investigation was that the elastic analysis allows to predict development of coup and contrecoup contusion within brain tissue against a frontal impact. From their comparison with previous experimental results [22], it is observed that the peak force value on the frontal bone was slightly higher. This may have been due to the fact that the scalp effect was not considered in that study, hence the scalp properties of Gilchrist [36] are applied in our first set of mechanical properties, which will be denoted as Model MP1.

The second model considered was developed by Ruan et al. [20] to study the dynamic response of the human head to direct impact by a rigid body, and to assess head impact severity from different types of impact. The brain and the scalp were considered as viscoelastic materials and the other head tissues were assumed to be elastic. In our simulations, viscoelastic materials will be defined by a Prony series expansion of the dimensionless relaxation modulus [15]:

$$g_R(t) = 1 - \sum_{i=1}^{N} \bar{g}_i{}^P (1 - e^{-t/\tau_i{}^G}) \tag{1}$$

where t stands for time, $\bar{g}_i{}^P$ and $\tau_i{}^G$ stand for material constants with $i = 1,2,\dots,N$. Ruan et al. [20] stated that the viscoelastic behaviour of the scalp was scaled from Galford and McElhaney [37], where a series of creep and relaxation experiments on monkey scalp are described, but the values are not provided. As the scalp properties are unknown, a linear-elastic behaviour has been assumed in the Model MP2 such as the one presented in Ruan and Prasad [38]. A drawback of this study of Ruan et al. [20] is that the FE model was validated for intracranial pressure data [22], like most human head FE models, and then used to predict brain injury. This is not convenient because it has been proved that the brain injury models that are validated for pressure alone (without considering brain motion and intracerebral acceleration) can give a wide range of shear responses to the same impact [39].

The third model considered was generated by Kleiven [35] to analyse the influence of inertial forces on the human head. This model is quite complete and includes some parts that have not been considered in the present study, such as the bridging veins, falx or meninges. A Mooney-Rivlin hyperelastic constitutive law was used for the central nervous system to account for the large elastic deformations, and the other head components were made of elastic material. The form of the Mooney-Rivlin strain energy density function is [40,41]:

$$W = C_{10}(\bar{I}_1 - 3) + C_{01}(\bar{I}_2 - 3) \quad (2)$$

where C_{10} and C_{01} stand for material parameters, $\bar{I}_1$ and $\bar{I}_2$ stand for the first and second deviatoric strain invariants. Sliding contact definitions were used to model the presence of CSF between the meningeal membranes and the brain, but the values are not provided so our Model MP3 does not include them. The head model of Kleiven [35] was validated against experimental data for intracranial pressure and brain motion. It was observed that the intracranial response is highly affected by the impact direction, and that low frequency rotation dynamics (with a long impulse duration) increases the strain level more than a high frequency impact for the same rotational acceleration amplitude.

The fourth model was developed by Kang et al. [12] in order to replicate a real head impact in motorcycle accident. This model includes the tentorium and falx to separate the cerebrum and cerebellum and the two hemispheres, but both cerebrum and cerebellum were modelled with the same mechanical properties. Viscoelastic properties were considered for the brain, and the other parts were assumed to be of elastic material. This model was validated for intracranial pressure, and then compared with the results from the accident reconstruction carried out by means of an instrumented Hybrid II headform and new helmets of the same manufacturer and model. It was shown that the model is able to predict the brain injury sites observed in the autopsy, although it slightly underestimates the maximum stresses. The Young's modulus (E) and Poisson's ratio (ν) of the brain are not given, although the bulk modulus (K) is provided. Therefore, in our Model MP4 several values of ν (between 0.4999 and 0.49999) have been considered, keeping K constant, and E has been calculated from them.

The last model was created by Tse [25] aiming to predict the mechanical response of the human head during a head injury. This model is fairly detailed in the definition of the various parts of the brain, however the cranium is not subdivided into different layers. It adopted linear viscoelastic material behaviour combined with the large-deformation theory for brain tissues, and a linear elastic material behaviour for the rest of parts. This model was validated against short and long duration impact experimental data and localized brain motion data.

2.3. Model calibration

Although the physical complexion of the subject (such as the thickness and curvature of the skull) may clearly influence the results, our model has been calibrated using some of the cadaveric experimental tests available in the literature. Firstly, we reproduced a dynamic experiment carried out by Yoganandan et al. [8] with our model in Abaqus/Explicit [15], see Section 2.3.1. This simulation helped us to calibrate the threshold values of stress of the skull and the scalp, and to decide between the element deletion technique and the mechanical properties degradation technique to deal with fracture. In both cases, the element will be either eliminated or its properties will be degraded considering the maximum normal stress criterion (Rankine's criterion), which states that failure occurs in a multiaxial state when:

$$\sigma_1 \geq \sigma_{ut} \quad or \quad \sigma_3 \leq \sigma_{uc} \tag{3}$$

where σ_1, σ_2 , and σ_3 stand for the principal stresses (considering $\sigma_1 \geq \sigma_2 \geq \sigma_3$), σ_{ut} stands for the uniaxial tensile strength, and σ_{uc} stands for the uniaxial compressive strength (considered negative). Secondly, we replicated a cadaveric study performed by Nahum et al. [22] (see Section 2.3.3) in order to have a better understanding of the mechanical behaviour of the brain and CSF. There are some limitations and uncertainties for the latter reference experiment, for instance, the diameter of the impactor and the mechanical properties of the impactor padding are unknown, being necessary to calibrate the simulation.

After calibrating the FE model, these experimental impact tests are used again as ground truth to analyse the behaviour of the different constitutive models and elastic constants provided in Table 1, in order to find the model that agrees with the experimental data in a better way.

2.3.1. Experimental test of Yoganandan et al. [8]

Yoganandan et al. [8] conducted a series of quasi-static and dynamic impact tests on twelve unembalmed intact human cadaver heads in order to delineate the biomechanics of skull fracture in different regions of the skull. Dynamic tests consisted of a hydraulic piston travelling at constant vertical velocity and impacting the head at a specific site until skull fracture. Force and deflection time histories were recorded. In order to calibrate the threshold values of the ultimate strength of the skull and the scalp, the dynamic test nº7 of Yoganandan et al. [8] has been replicated in this

work because of the similarity between the subject's physical complexion. The 48-mm semispherical anvil has been modelled as a rigid body which hits the head vertically at a constant velocity of 7.2 ms^{-1}. The head model developed in this work was placed on a flat surface, thus constraining vertical displacement, and also pinned near the ears as depicted in Fig. 3.

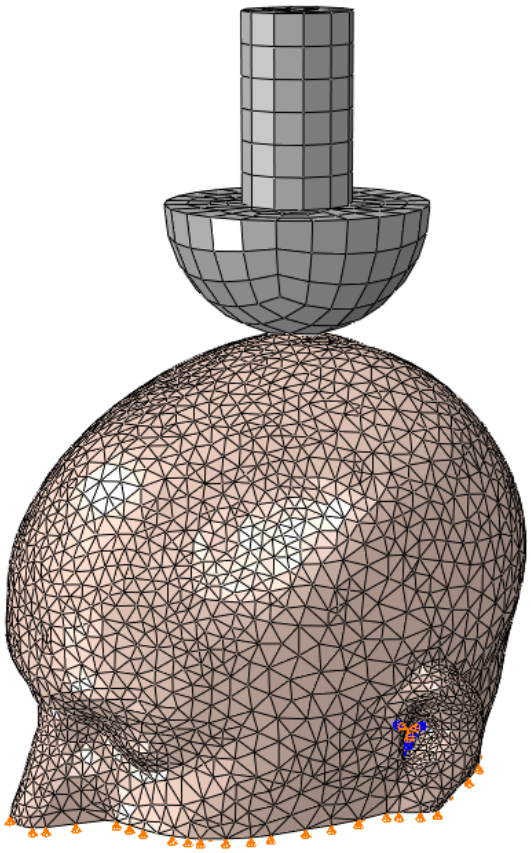

Fig. 3. Yoganandan's et al. [8] experiments replication setup with our FE model.

The available data in the literature about the mechanical behaviour of the scalp is scarce. Some fresh human scalp specimens were tested in compression by Melvin et al. [42] and a series of relaxation tests in tension on monkey scalp specimens were performed by Galford and McElhaney [37]. From the compression tests, it is observed that the scalp tissue behaviour is almost linearly elastic (E = 16.7 MPa) until strains of 30-40% are reached, but the fracture limit strain (ε_u) is unknown. Therefore, several simulations were run in this work by varying this limit strain value of the scalp to delete the scalp elements and then applying the same mechanical properties for the rest of head tissues. Model MP1 was used, although any other could be used, in order to select the most appropriate strain limit. The results of these simulations can be seen in Fig. 4, where the force exerted by the piston versus its displacement was plotted for different

values of the critical strain. In particular, for 60%, 65% and 70%. It is observed that the most appropriate strain limit is 70% because its force-deflection curve is the most similar to the experimental behaviour, given by the black dashed line corresponding to the experimental data provided by Yoganandan et al. [8].

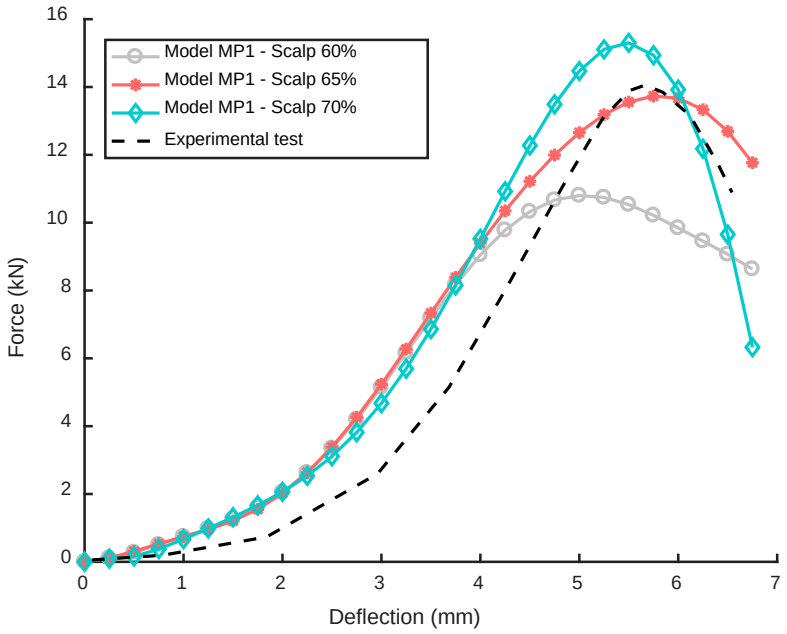

Fig. 4. Scalp ultimate strain calibration.

On the other hand, it is possible to find some studies that provide threshold values of the skull bone ultimate strength. Table 2 shows some of them. In order to choose a threshold value of the skull bone ultimate strength for our model, a comparative study was carried out for all the constitutive models. The simulation of the Yoganandan's et al. [8] experiment was performed with each of the different threshold values of the ultimate strength provided in Table 2, i.e. a total of 20 simulations. The same trend is observed for the first four constitutive models, where Sahoo et al. [43] fits slightly better to the experimental data than the rest of force-deflection curves and it is more conservative. To exemplify, the obtained results for the Model MP2 are shown in Fig. 5. However, Silver [44] fits better the experimental results for the Model MP5. Silver [44] provides a limit value for the skull as a whole, which is in line with the simplification of making no distinction between compact bone and diploë assumed by Tse [25]. Hence, the ultimate stress threshold values for compact bone are very conservative and remain on the safety side, although for cancellous bone are not as conservative as for the other four models. Therefore, the threshold

values of Sahoo et al. [43] have been selected for the first four models and Silver [44] for the Model MP5 for the rest of the analysis.

Table 2: Ultimate Compressive and Tensile Stress threshold values for bone tissues.

	Compact bone		**Diploë**		**Skull***	
	σ_{uc} **(MPa)**	σ_{ut} **(MPa)**	σ_{uc} **(MPa)**	σ_{ut} **(MPa)**	σ_{uc} **(MPa)**	σ_{ut} **(MPa)**
Raul et al. [45]	-145	90	-28	35		
Sahoo et al. [43]	-132	90	-24.8	34.8		
Evans and Lissner [46]	-152.2,-167.4	70.5	-25.1	-		
Silver [44]					-85	42.5

*No distinction is made between compact bone and diploë

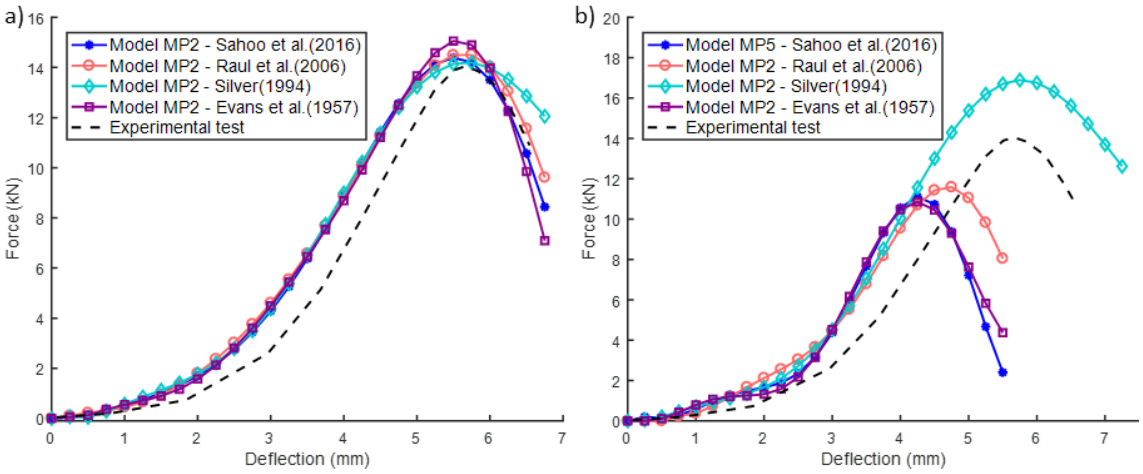

Fig. 5. Comparison among the ultimate threshold values for bone tissues of Table 2 for:

a) Model MP2 b) Model MP5.

Once the critical values are chosen, we proceed to analyse both the response of the element removal technique and the property degradation technique for all models. In both cases a VUSDFLD subroutine [47] was defined. For the second technique, the Young's moduli are reduced to a significantly low value. With this method the information and properties like mass of the failed elements are not lost in their elimination and it is easier to observe the fracture. The response was similar for all five models. As shown in Fig. 6, the force-deflection curve obtained in the experimental replication for the properties degradation case varies little when compared to the no change in properties case. The curve slope is practically the same as that obtained without changing the properties, although, the peak force is lower. This curve slope is higher than that obtained by the element deletion technique and is outside the range of values of the experiments. Furthermore, in the case of property degradation, the simulation aborts shortly after starting to surpass the limit in a very small number of elements of the compact bone. However, the force-

deflection curve provided by the element deletion technique provides a response more similar to the experimental one. Therefore, although a priori it may seem that the removal of elements is an unrealistic technique, the element deletion technique performs better and it will be used in the rest of the study.

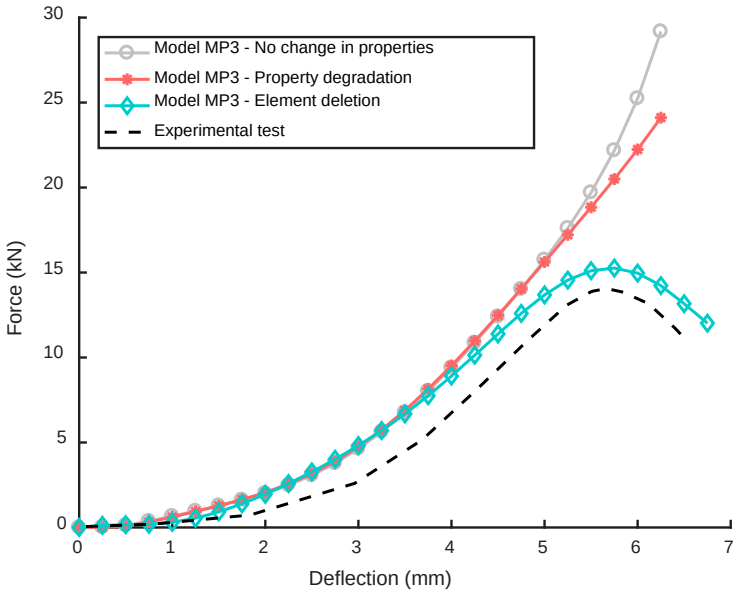

Fig. 6. Comparison between the element deletion and property degradation techniques.

As mentioned in Section 0, Kang et al. [12] do not provide E and ν. Hence for Model MP4, three values of ν have been considered and E has been calculated from them (keeping K constant). The differences are slight since the range of variation of ν is small, and there is no clear pattern of influence (see Fig. 7).

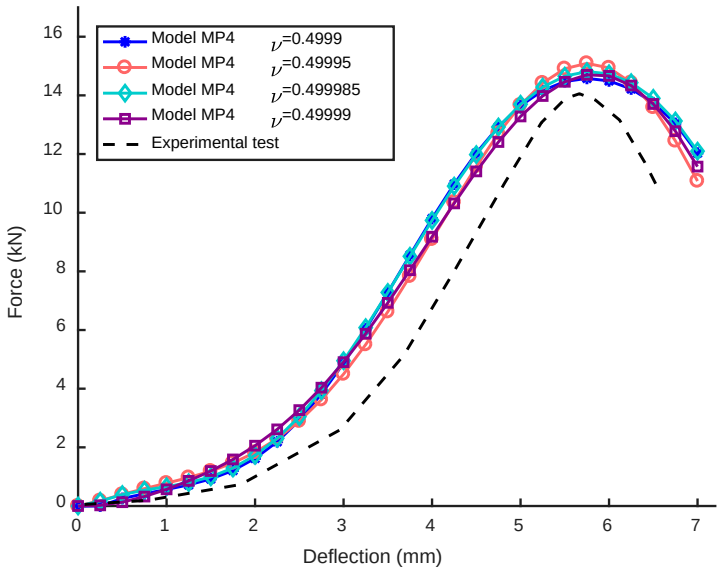

Fig. 7. Sensitivity to Poisson's ratio variations.

2.3.2. Experimental test of Nahum et al. [22]

This is the most widely known cadaveric study, where two series of head impact experiments were carried out to correlate intracranial pressures with other impact parameters. In Nahum et al. [22], Series I consisted of individual experiments and Series II consisted of multiple sequential impacts on a single individual. Histories of force and acceleration of the head gravity centre were recorded, and pressure at different locations inside the cranium were measured. The unembalmed specimens were prepared in order to simulate realistic fluid pressures within the CSF space and cerebral blood vessels. The specimen is seated in such a way that the impactor strikes the forehead making an angle of 45º angle with respect to its Frankfort anatomical plane. Suture attachments were placed to each ear in order to maintain the head's position without inhibiting anterior-posterior movement of the head during the impact loading.

In our study, Series I experiment nº 37 is chosen for comparison because it is the one for which more results are provided, including the input force, head acceleration and intracranial pressure curves. The specimen was impacted by a rigid mass of 5.59 kg travelling at a constant velocity of 9.94 m/s. A padding layer is included in order to control the impulse duration. The dimensions of the striking body and the mechanical properties of the padding material are not provided by Nahum et al. [22]. Consequently, our simulation (see Fig. 8) was calibrated by adjusting the dimensions of the impactor, stiffness of the foam padding and setting adequate boundary conditions and a velocity history for the impactor such that the resulting input force fits the experimental results (see Fig. 9a). The resulting acceleration in the head was measured on the skull temporal lobe centroid. It matches the evolution stated by Nahum et al. [22], as can be seen in Fig. 9b, so we can conclude that the impact conditions are properly determined. As a result of the good agreement with the response given by Nahum et al. [22], we consider our head model validated for the rest of the study.

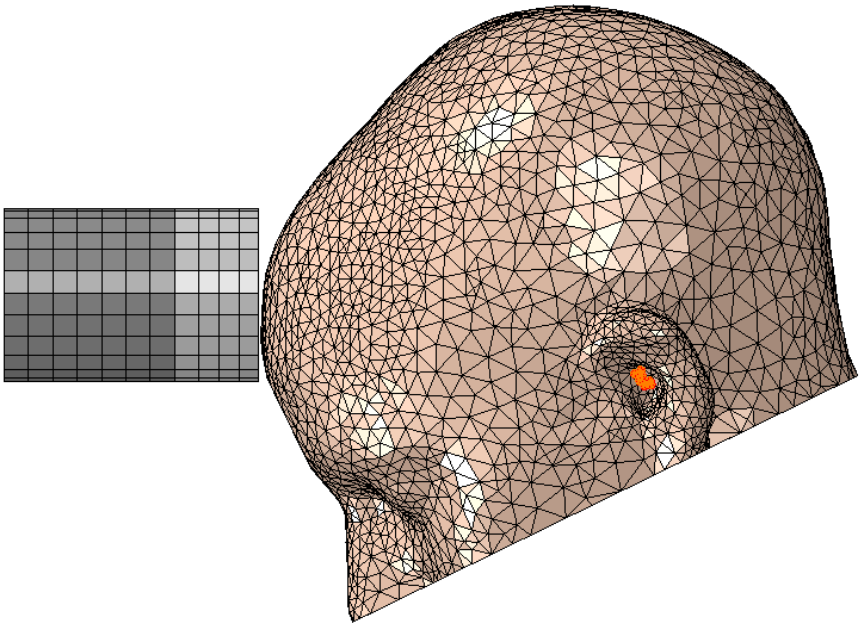

Fig. 8. Nahum's et al. [22] experiment replication setup with our FE model.

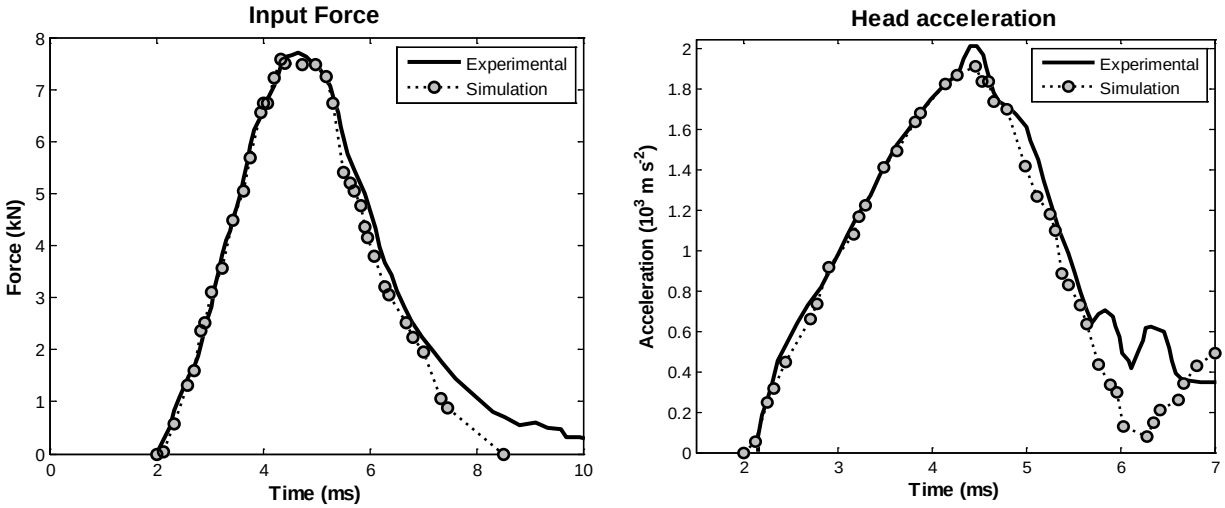

Fig. 9. a) Input force history in experiment nº37 of Nahum et al. [22] and the one obtained in this work, b) Acceleration history for both experiment and simulation.

3. Skull fracture

Once the model was calibrated, a comparative study of the different constitutive models reviewed in Section 2.2 was carried out by simulating again the Yoganandan's et al. [8] experimental test. Fig. 10 shows the results of the force-deflection curves obtained by these models together with the experimental test curve. It can be observed that all the material models considered in our simulation give a similar response. This response involves a first stage of non-linearity corresponding to the damping of the force due to scalp energy absorption, followed by a linear

portion where stiffness properties can be estimated, and finally another non-linear part corresponding to the skull fracture. The scalp of the specimen #7 [8] was 2 mm thicker than our FE model, thus the force damping that takes place in the scalp in the first stage of the dynamic test is considerably lower in the simulation. Consequently, the reaction force of the simulation curves start to grow earlier than in the Yoganandan's et al. [8] experimental curve.

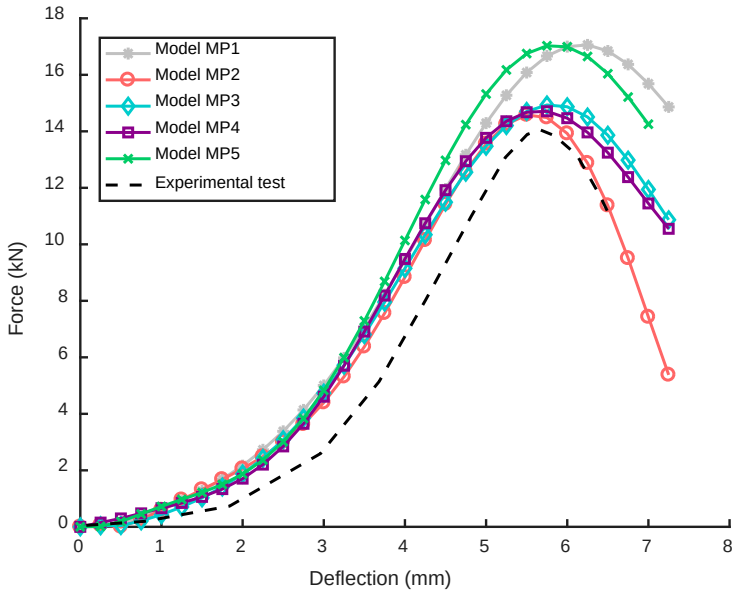

Fig. 10. Force-deflection response of the different mechanical properties.

In the impact region, the outer table of the skull is subjected to compression and the inner table is subjected to tensile stresses. Although the compact bone is more prone to failure due to tension than compression, the rupture occurs in the outer layer since the local stresses are very high. This initial damage to the outer table of the calvarium coincides with the one indicated by Yoganandan et al. [8]. Fracture appeared last in the Model MP1 since the compact bone stiffness is the lowest among the models (E=5465 MPa, Table 1). It was expected that Models MP3 and MP4 would fracture first because they present the highest stiffness (E=15000 MPa, Table 1), however, this does not happen. This means that the diploë also influences the rupture. The Model MP2 fractures before Models MP3 and MP4, although its compact bone stiffness (E=12200 MPa, Table 1) is slightly lower than that of the Models MP3 and MP4, but the diploë stiffness is the highest (E=5660 MPa, Table 1) among the four models developed using the same stress threshold values ([43]; Table 2). The diploë thickness reduces the deflection, increasing the overpressure and favouring fracture. Likewise, although Models MP3 and MP4 have the same compact bone stiffness, Model MP4 fractures first than Model MP3 because its diploë Young's

modulus is higher (E=4500 MPa and E=1000 MPa respectively, Table 1). Therefore, the value of the displacement at failure is strongly dependent on the moduli of elasticity of both skull bones, in such a way that increasing the values of E leads to an earlier fracture. The behavior of the Model MP5 cannot be taken into account for this comparison of the elastic constants, since it has been developed using different stress threshold values ([44]; Table 2). On the other hand, the values of the elastic constants for the skull bones of models MP1 and MP5 would be the most conservative and, on the contrary, Model MP2 constants would be the least conservative under these conditions.

The stiffness of the structure, defined as the slope of the force-deflection response in the linear region, ranged from 2462 to 5867 N/mm for dynamic loading tests of Yoganandan et al. [8]. All the stiffness values obtained in the different simulations are within this range (see Table 3). Therefore, taking into account the stiffness and the peak force of the different models, the Model MP4 tends to represent the fracture behaviour of the experiment in a better way than the rest of material models.

Table 3.Comparison of the stiffness for the different mechanical properties.

Mechanical Properties	Stiffness (N/mm)
1	4938.8
2	5065.3
3	4671.5
4	4932.7
5	5655.9
Experiment	4798.0

4. Intracranial pressure response

The simulation of the experimental test carried out by Nahum et al. [22] was performed for the five material models, taken from literature (Table 1) and developed in Section 3, with the purpose of getting a relationship between intracranial pressure responses and elastic properties of brain and CSF. Pressure time histories were taken upon the external surface of the brain, in the four locations shown in Fig. 11, and compared against the experimental values. Nahum et al. [22] used pressure transducers inserted in a perforation through the thickness of the cranium, and the depth of penetration of the transducer is not specified, thus some measurements could have been taken in the cerebrospinal fluid region. Results of the comparison are shown in Fig. 12.

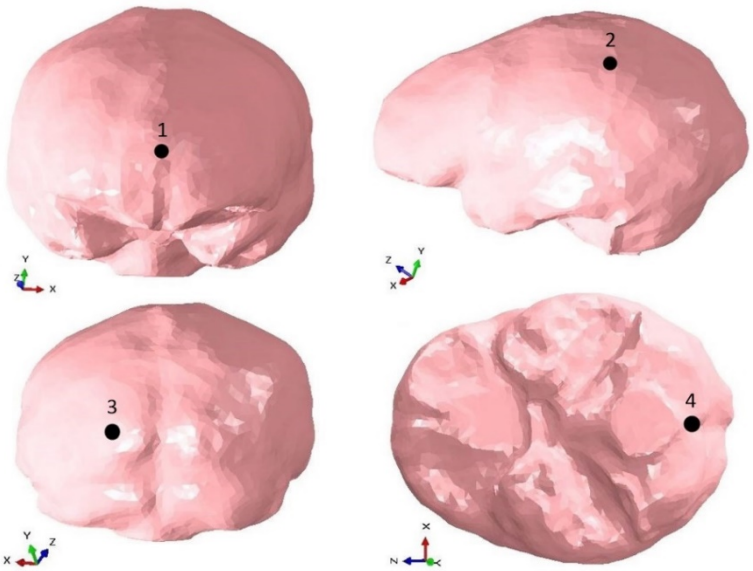

Fig. 11. Pressure measurement sites: 1) Frontal, 2) Parietal region, 3) Occipital, 4) Posterior fossa

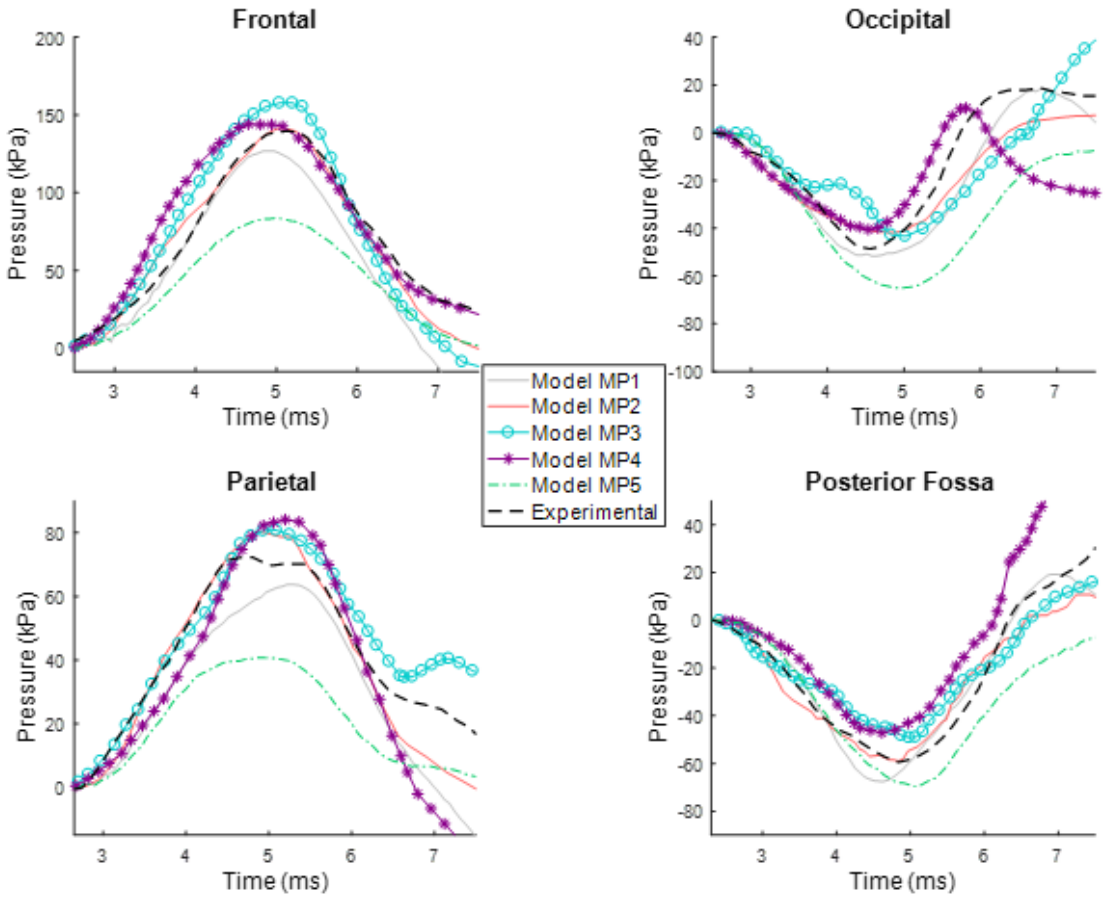

Fig. 12. Intracranial pressure response for the experiment and simulations.

Pressure measurement has proved to be very sensitive to the value of the bulk modulus of the brain, as stated by Ruan et al. [48] who showed that an increase in *K* led to higher positive

pressures and decreased the magnitude of the negative ones. Gilchrist and O'Donoghue [23] suggested that because of the heterogeneous composition of the brain, it should be considered as a gelatine rather than purely water. This statement involved a decrease in ν as a reduction in water content (incompressible). Results obtained in this work reveal that the least compressible brain model, corresponding to Model MP5 (ν=0.48, Table 1), underpredicts frontal and parietal pressure values when compared to the experimental values, while overpredicts the corresponding to the occipital lobe and posterior fossa (see Fig. 12). Nonetheless, there are no viscoelastic properties available for this model so the impact damping is lower. This fact can result in greater peak values. If a high bulk modulus is chosen (Models MP2, MP3 and MP4), pressure curves shift towards more positive values until the incompressibility limit is reached.

The influence of CSF mechanical properties on intracranial pressure has been discussed in previous studies [49,50], which conclude that the elastic constants defined for this fluid do not play a determinant role in pressure response. Nevertheless, the initial simulations performed in our analyses using Model MP4 revealed a pressure distribution across brain tissue which is not consistent with the other models. The cause of this discrepancy is the initial assumption of a low elastic modulus for CSF (E=12 kPa, Table 1). For this reason, it has been replaced a posteriori by values which are one and two orders of magnitude higher (E=120 kPa and E=1.2 MPa) resulting in a substantial improvement in pressure results.

In Fig. 13, complete pressure distribution contours along the brain at time 4.5 ms reveal the differences between the constitutive models applied. The most compressible models (Fig. 13a, f) have highly linear response in the propagation of pressure perturbation along impact direction. Therefore, time curves are smooth as opposed to the almost incompressible models (Fig. 13c, d, e) that present an oscillatory behaviour noticeable in Fig. 12. It is probably magnified by the FE calculation method, that becomes unstable when dealing with Poisson's coefficients greater than 0.49995. Pressure contours of Model MP4 (Fig. 13d) have a wider range due to stress concentration in brain protuberances. This fact, that is negligible in the other analysis performed, becomes relevant for this case because the CSF elastic modulus is still low, despite having incremented its initial value by an order of magnitude (E=120 kPa). However, when modifying the initial assumption of Kang et al. [12] by two orders of magnitude and taking E=1.2 MPa, the distribution becomes more realistic and in agreement with the rest of results (Fig. 13e).

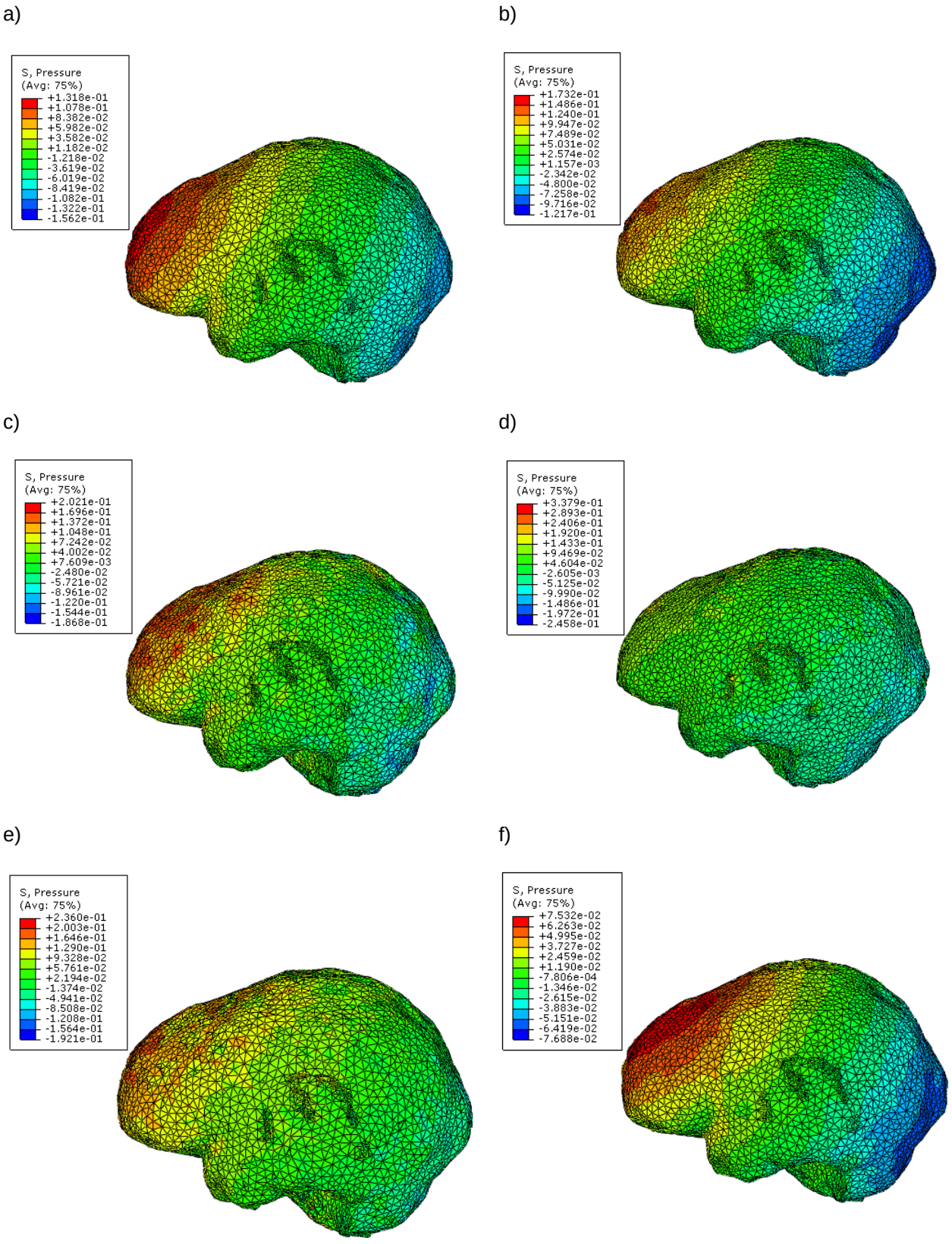

Fig. 13. Pressure contours at t=4.5 ms for a) Model MP1, b) Model MP2, c) Model MP3, d) Model MP4 with E=120 kPa for CSF e) Model MP4 with E=1.2 MPa for CSF, e) Model MP5.

In view of the obtained results, a non-linear viscoelastic behaviour (Model MP2) with high K matches the experimental results with less error than other models. However, this kind of constitutive model is not the most suitable for soft tissues, where a hyperelastic model based on the strain energy function is preferred (Model MP3).

As the response obtained with the hyperelastic Model MP3 presented here seems not so accurate predicting the experimental intracranial pressure values, the influence of parameter K for this model has been analysed in order to obtain the closest fit to the experimental results of Nahum et al. [22]. One problem that arises when dealing with nearly-incompressible hyperelastic materials in FE explicit analysis is the need for high accuracy with very low time increments. Results in Fig. 14 have been obtained by performing double-precision Abaqus/Explicit simulations. The previously described trend of increasing positive pressure when approaching to incompressibility can be clearly appreciated. The best correlation with experimental data is achieved with a bulk modulus of 0.21 GPa, one order of magnitude less than the one for water. This fact supports the assumption that brain is not an entirely incompressible fluid-like material [23,50].

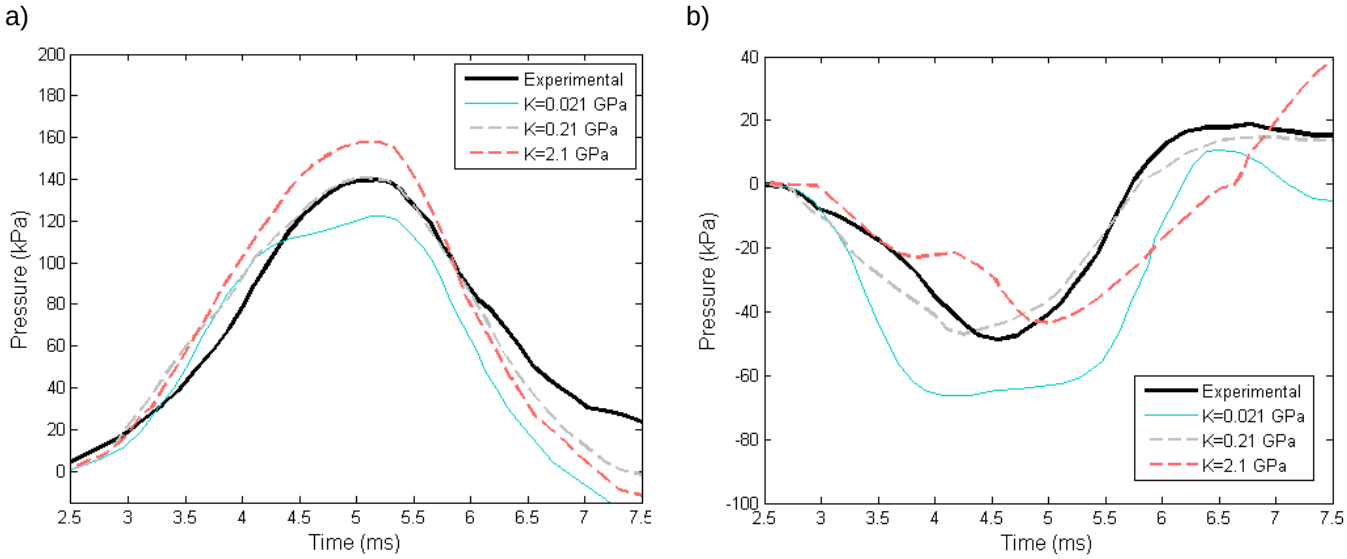

Fig. 14. Sensitivity analysis of brain K over intracranial pressure for our Model MP3 by means of the experiment performed by Nahum et al. [22]: a) frontal pressure, b) occipital pressure.

Beyond the analysis presented in this study, it is known that the brain response is fairly strain rate dependent and the extension of the model proposed here over a wide range of problems should take into account this strain rate dependency. Additionally, although the homogenization

considered here yields good results, the heterogeneous nature of brain tissue could also be considered in more refined models.

5. Conclusions

The results obtained throughout the different analyses show that the methodology followed allows the reproduction of experimental results. To the best of the authors' knowledge, no previous study has compared the different constitutive models neither the influence of the different values of elastic constants shown in literature with the same FE model against experimental impact tests. Despite the discrepancies between material models, all stiffness values obtained are within the range of cadaveric dynamic tests and the intracranial pressures follow the same trend.

The main conclusions can be summarized as follows:

- The most appropriate ultimate strain value is 70% because its force-deflection curve is the most representative when compared to experimental behaviour.
- Appropriate ultimate compressive and tensile stress threshold values were proposed.
- The technique of element deletion applying Rankine failure criterion is appropriate to deal with fracture.
- Compact bone has proved to be critical in skull fracture but it has been shown that there are other tissues (like the diploë) that also have a considerable influence.
- CSF constitutive properties have been considered in other studies not to be determinant in pressure response in the brain, but results obtained in this work show that the elastic properties of this fluid actually affect the intracranial pressure distribution. The choice of E~1 MPa provides results close to experimental data, while lower values make the response become unstable.
- The consideration of brain tissue as a nearly-incompressible solid with a high (but not complete) water content offers pressure responses consistent with experimental data on post-mortem human. Hyperelastic/viscoelastic modelling of the brain with a bulk modulus value of 0.21 GPa gives the closest approach.

Aknowledgements

The authors thank the financial support received from the Spanish Ministry of Economy and Competitiveness and the FEDER operation program through the project RTC-2015-3887-8. The support of the Generalitat Valenciana through the program PROMETEO 2016/007 is also acknowledged.

References

1. Hyder AA, Wunderlich CA, Puvanachandra P, Gururaj G, Kobusingye OC. The impact of traumatic brain injuries: a global perspective. *NeuroRehabilitation* 2007; **22**(5):341–53.http://www.ncbi.nlm.nih.gov/pubmed/18162698AccessedOctober 20, 2016.

2. Meaney DF, Morrison B, Dale Bass C. The Mechanics of Traumatic Brain Injury: A Review of What We Know and What We Need to Know for Reducing Its Societal Burden. *Journal of Biomechanical Engineering* 2014; **136**(2):21008. doi:10.1115/1.4026364.

3. WHO Report. Violence and Injury Prevention and Disability (VIP) - Neurotrauma. WHO 2010. http://www.who.int/violence_injury_prevention/road_traffic/activities/neurotrauma/en/. Accessed October 21, 2016.

4. Deng X, Potula S, Grewal H, Solanki KN, Tschopp MA, Horstemeyer MF. Finite element analysis of occupant head injuries: Parametric effects of the side curtain airbag deployment interaction with a dummy head in a side impact crash. *Accident Analysis & Prevention* 2013; **55**:232–241. doi:10.1016/j.aap.2013.03.016.

5. Marjoux D, Baumgartner D, Deck C, Willinger R. Head injury prediction capability of the HIC, HIP, SIMon and ULP criteria. *Accident Analysis & Prevention* 2008; **40**(3):1135–1148. doi:10.1016/j.aap.2007.12.006.

6. Bolander R, Mathie B, Bir C, Ritzel D, VandeVord P. Skull flexure as a contributing factor in the mechanism of injury in the rat when exposed to a shock wave. *Annals of biomedical engineering* 2011; **39**(10):2550–9. doi:10.1007/s10439-011-0343-0.

7. Li G, Zhang J, Wang K, Wang M, Gao C, Ma C. Experimental research of mechanical behavior of porcine brain tissue under rotational shear stress. *Journal of the Mechanical Behavior of Biomedical Materials* 2016; **57**:224–234. doi:10.1016/j.jmbbm.2015.12.002.

8. Yoganandan N, Pintar FA, Sances A, et al. Biomechanics of skull fracture. *Journal of neurotrauma* 1995; **12**(4):659–68. doi:10.1089/neu.1995.12.659.

9. Motherway JA, Verschueren P, Van der Perre G, Vander Sloten J, Gilchrist MD. The mechanical properties of cranial bone: The effect of loading rate and cranial sampling position. *Journal of Biomechanics* 2009; **42**(13):2129–2135. doi:10.1016/j.jbiomech.2009.05.030.

10. Lakatos É, Magyar L, Bojtár I. Material Properties of the Mandibular Trabecular Bone. *Journal of Medical Engineering* 2014; **2014**:1–7. doi:10.1155/2014/470539.

11. Simpleware Ltd. ScanIP Reference Guide Version 4.2. 2010.

12. Kang H-S, Willinger R, Diaw BM, Chinn B. Validation of a 3D anatomic human head model and replication of head impact in motorcycle accident by finite element modeling. In: *Stapp Car Crash Conference Proceedings*; 1997.

13. Tse KM, Tan L Bin, Lee SJ, Lim SP, Lee HP. Investigation of the relationship between facial injuries and traumatic brain injuries using a realistic subject-specific finite element head model. *Accident Analysis & Prevention* 2015; **79**:13–32. doi:10.1016/j.aap.2015.03.012.

14. Horgan TJ, Gilchrist MD. The creation of three-dimensional finite element models for simulating head impact biomechanics. *International Journal of Crashworthiness* 2003; **8**(4).

15. Dassault Systèmes. *Abaqus 6.12 User's Manual*.; 2012.

16. Dassault Systèmes. Abaqus Example Problems Manual, 2.1.3 Rigid projectile impacting eroding plate. 2012:1–5.

17. Kleiven S, Von Holst H. Consequences of head size following trauma to the human head. *Journal of Biomechanics* 2002; **35**(2). doi:10.1016/S0021-9290(01)00202-0.

18. Zhou C, Khalil TB, King AI. A new model comparing impact responses of the homogeneous and inhomogeneous human brain. In: *SAE Technical Papers*; 1995.

19. Willinger R, Taleb L, Kopp CM. Modal and temporal analysis of head mathematical models. *Journal of Neurotrauma* 1995; **12**(4):743–754.

20. Ruan JS, Khalil TB, King AI. Finite element modeling of direct head impact. *SAE Technical*

Papers 1993. doi:10.4271/933114.

21. Tan L Bin, Chew FS, Tse KM, Chye Tan VB, Lee HP. Impact of complex blast waves on the human head: a computational study. *International Journal for Numerical Methods in Biomedical Engineering* 2014; **30**(12):1476–1505. doi:10.1002/cnm.2668.

22. Nahum AM, Smith R, Ward CC. Intracranial pressure dynamics during head impact. In: *SAE Technical Papers*; 1977.

23. Gilchrist MD, O'Donoghue D. Simulation of the development of frontal head impact injury. *Computational Mechanics* 2000; **26**(3):229–235.

24. Shugar TA, Katona MG. Development of finite element head injury model. *ASCE Journal of the Engineering Mechanics Division* 1975; **101**(3):223–239.

25. Tse KM. Development of a Realistic Finite Element Model of Human Head and its Applications to Head Injuries. 2013.

26. Willinger R, Kang HS, Diaw B. Three-dimensional human head finite-element model validation against two experimental impacts. *Annals of Biomedical Engineering* 1999; **27**(3):403–410.

27. Yang B, Tse K-M, Chen N, et al. Development of a finite element head model for the study of impact head injury. *BioMed research international* 2014; **2014**:408278. doi:10.1155/2014/408278.

28. Mendis KK, Stalnaker RL, Advani SH. A constitutive relationship for large deformation finite element modeling of brain tissue. *Journal of Biomechanical Engineering* 1995; **117**(3):279–285.

29. Sahoo D, Deck C, Willinger R. Development and validation of an advanced anisotropic visco-hyperelastic human brain FE model. *Journal of the Mechanical Behavior of Biomedical Materials* 2013; **33**:24–42. doi:10.1016/j.jmbbm.2013.08.022.

30. Belingardi G, Chiandussi G, Gaviglio I. Development and validation of a new finite element model of human head. In: *Proceedings of 19th International Technical Conference on the Enhanced Safety of Vehicles.* Washington, USA; 2005.

31. Tse KM, Tan L Bin, Lee SJ, Lim SP, Lee HP. Development and validation of two subject-specific finite element models of human head against three cadaveric experiments. *International*

Journal for Numerical Methods in Biomedical Engineering 2014; **30**(3):397–415. doi:10.1002/cnm.2609.

32. Yang J. Investigation of Brain Trauma Biomechanics in Vehicle Traffic Accidents Using Human Body Computational Models. In: *Computational Biomechanics for Medicine*. New York, NY: Springer New York; 2011:5–14.

33. Mao H, Gao H, Cao L, Genthikatti VV, Yang KH. Development of high-quality hexahedral human brain meshes using feature-based multi-block approach. *Computer Methods in Biomechanics and Biomedical Engineering* 2013; **16**(3):271–279. doi:10.1080/10255842.2011.617005.

34. Yan W, Pangestu OD. A modified human head model for the study of impact head injury. *Computer Methods in Biomechanics and Biomedical Engineering* 2011; **14**(12):1049–1057. doi:10.1080/10255842.2010.506435.

35. Kleiven S. Evaluation of head injury criteria using a finite element model validated against experiments on localized brain motion, intracerebral acceleration, and intracranial pressure. *International Journal of Crashworthiness* 2006; **11**(1):65–79. doi:10.1533/ijcr.2005.0384.

36. Gilchrist MD. Modelling and accident reconstruction of head impact injuries. In: *Key Engineering Materials*, vol 245–246. Trans Tech Publications Ltd; 2003:417–430.

37. Galford JE, McElhaney JH. A viscoelastic study of scalp, brain, and dura. *Journal of Biomechanics* 1970; **3**(2):211–221. doi:10.1016/0021-9290(70)90007-2.

38. Ruan JS, Prasad P. Study of the biodynamic characteristics of the human head. In: *International IRCOBI conference on the biomechanics of impact*. Dublin; 1997:63–74.

39. Bradshaw D, Morfey C. Pressure and shear response in brain injury models. *Proceedings of the 17th International Technical Conference on the Enhanced Safety of Vehicles* 2001:1–10.

40. Mooney M. A Theory of Large Elastic Deformation. *Journal of Applied Physics* 1940; **11**(9):582–592. doi:10.1063/1.1712836.

41. Rivlin RS. Large Elastic Deformations of Isotropic Materials. IV. Further Developments of the General Theory. *Philosophical Transactions of the Royal Society of London A: Mathematical,*

Physical and Engineering Sciences 1948; **241**(835).

42. Melvin JW, McElhaney JH, Roberts VL. Development of a mechanical model of the human head - Determination of tissue properties and synthetic substitute materials. In: *SAE Technical Papers*; 1970.

43. Sahoo D, Deck C, Yoganandan N, Willinger R. Development of skull fracture criterion based on real-world head trauma simulations using finite element head model. *Journal of the Mechanical Behavior of Biomedical Materials* 2016; **57**:24–41. doi:10.1016/j.jmbbm.2015.11.014.

44. Silver FH. *Biomaterials, Medical Devices and Tissue Engineering: An Integrated Approach*. Dordrecht: Springer Netherlands; 1994.

45. Raul J-S, Baumgartner D, Willinger R, Ludes B. Finite element modelling of human head injuries caused by a fall. *International Journal of Legal Medicine* 2006; **120**(4):212–218. doi:10.1007/s00414-005-0018-1.

46. Evans FG, Lissner HR. Tensile and Compressive Strength of Human Parietal Bone. *Journal of Applied Physiology* 1957; **10**(3).

47. Dassault Systèmes. Section 1.2.19 VUSDFLD, Abaqus User Subroutines Reference Manual. 2012.

48. Ruan JS, Khalil T, King AI. Dynamic response of the human head to impact by three-dimensional finite element analysis. *Journal of Biomechanical Engineering* 1994; **116**(1):44–50.

49. Chafi MS, Dirisala V, Karami G, Ziejewski M. A finite element method parametric study of the dynamic response of the human brain with different cerebrospinal fluid constitutive properties. *Proceedings of the Institution of Mechanical Engineers. Part H, Journal of engineering in medicine* 2009; **223**(8):1003–19.

50. Ruan J, Prasad P. The influence of human head tissue properties on intracranial pressure response during direct head impact. *International Journal of Vehicle Safety* 2006; **1**(4):281. doi:10.1504/IJVS.2006.011230.